HHS Public Access

Author manuscript

ACS Nano. Author manuscript; available in PMC 2018 April 20.

Published in final edited form as:

ACS Nano. 2015 March 24; 9(3): 2420–2432. doi:10.1021/nn504025a.

Avasimibe Encapsulated in Human Serum Albumin Blocks Cholesterol Esterification for Selective Cancer Treatment

Steve Seung-Young Lee[1,†], **Junjie Li**[2,†], **Jien Nee Tai**[3], **Timothy L. Ratliff**[4,5], **Kinam Park**[1,4,6], and **Ji-Xin Cheng**[1,3,4,*]

[1]Weldon School of Biomedical Engineering, Purdue University, West Lafayette, IN 47907

[2]Department of Biological Sciences, Purdue University, West Lafayette, IN 47907

[3]Department of Chemistry, Purdue University, West Lafayette, IN 47907

[4]Center for Cancer Research, Purdue University, West Lafayette, IN 47907

[5]Department of Comparative Pathobiology, Purdue University, West Lafayette, IN 47907

[6]Department of Industrial and Physical Pharmacy, Purdue University, West Lafayette, IN 47907

Abstract

Undesirable side effects remain a significant challenge in cancer chemotherapy. Here we report a strategy for cancer-selective chemotherapy by blocking acyl-CoA cholesterol acyltransferase-1 (ACAT-1)-mediated cholesterol esterification. To efficiently block cholesterol esterification in cancer *in vivo*, we developed a systemically injectable nanoformulation of avasimibe (a potent ACAT-1 inhibitor), called avasimin. In cell lines of human prostate, pancreatic, lung, and colon cancer, avasimin significantly reduced cholesteryl ester storage in lipid droplets and elevated intracellular free cholesterol levels, which led to apoptosis and suppression of proliferation. In xenograft models of prostate cancer and colon cancer, intravenous administration of avasimin caused the concentration of avasimibe in tumors to be 4-fold higher than the IC_{50} value. Systemic treatment of avasimin notably suppressed tumor growth in mice and extended the length of survival time. No adverse effects of avasimin to normal cells and organs were observed. Together, this study provides an effective approach for selective cancer chemotherapy by targeting altered cholesterol metabolism of cancer cells.

Graphical Abstract

[*]Corresponding author: Ji-Xin Cheng, Weldon School of Biomedical Engineering, 206 S. Martin Jischke Drive, West Lafayette, IN 47907, Tel: +1 765 494 4335; jcheng@purdue.edu.

[†]Equal contribution;

Author contributions

S.S.-Y.L., J.L., and J.N.T. performed experiments and analyzed data. S.S.-Y.L and J.X.C. designed the experiments and wrote the manuscript. T.L.R. and K.P. contributed to the experimental design and commented on the manuscript.

Competing Financial Interests: The authors declare no competing financial interests.

Supporting Information Available: Avasimin characterization and additional experimental figures. This material is available free of charge *via* the Internet at http://pubs.acs.org

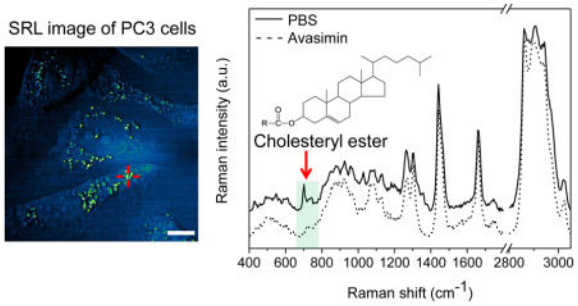

Keywords

ACAT-1 inhibitor; avasimibe; human serum albumin; cholesteryl ester; cholesterol; cancer

The metabolic pathways of cancers have recently been recognized as novel targets for selective chemotherapy because proliferating cancer cells exhibit remarkably distinct metabolic requirements compared to the normal differentiated cells.[1–3] In particular, altered lipid metabolism including cholesterol is an emerging target for aggressive cancers.[4–8] Since cholesterol is an essential component for the cell membrane and for signaling molecule synthesis, cancer cells require large amounts of cholesterol for their development and growth.[9] Lipid metabolic reprogramming allows cancer cells not only to obtain substantial cholesterol through low-density lipoprotein (LDL) uptake and *de-novo* biosynthesis[10] but also to accumulate cholesterol into their intracellular lipid reservoir, namely lipid droplets, after converting cholesterol to cholesteryl esters.[11] Because high intracellular cholesterol levels induce cytotoxicity, cholesterol esterification by acyl-CoA cholesterol acyltransferase-1 (ACAT-1) is a key process in cells.[12] Blocking ACAT-1 activity by inhibitors reduced levels of cholesteryl esters in cancer cells and suppressed cancer proliferation with no obvious negative effects to normal cells.[13–16] These results show great potential of targeting ACAT-1 for cancer-selective therapy. Notably, a number of ACAT-1 inhibitors have been developed as hypolipidemic and anti-atherosclerotic drugs.[17, 18] However, almost all inhibitors are hydrophobic compounds which were administered orally to target hepatic ACAT-derived cholesteryl esters such as very low density lipoprotein (VLDL), resulting in low blood-bioavailability of the inhibitors.[19–21] Although intraperitoneal administration of an ACAT-1 inhibitor, avasimibe, in DMSO with a surfactant has shown anti-tumor effects, this method is inappropriate for clinical application.[7] Therefore, to repurpose ACAT-1 inhibitors as cancer chemotherapy agents, a formulation that effectively and safely delivers the inhibitor to the tumor is essential.

Here we report a systemically injectable and clinically viable nanomedicine which targets ACAT-1 and depletes cholesteryl esters for selective cancer chemotherapy. We employed a potent ACAT-1 inhibitor, avasimibe,[22–24] and encapsulated it with human serum albumin (HSA) to create a highly water-soluble nano-sized formulation, named as avasimin. Using label-free Raman spectromicroscopy, we determined the cholesteryl ester-depletion capacity of avasimin for different human cancer cell lines. Furthermore, we characterized the blood-bioavailability and tissue-distribution of avasimibe following intravenous administration of avasimin. The anti-tumor effects and survival benefits of avasimin in mouse models of

human prostate and colon cancers were demonstrated. *In vivo* safety of avasimin was shown through hematological and histological analyses, and through evaluation of lipid droplet compositions in lipid-rich organs such as liver and adrenal glands.

Results

Water-soluble avasimibe formulation

To develop an injectable and cancer-selective avasimibe formulation, we utilized human serum albumin (HSA) due to its high biocompatibility and binding capability for hydrophobic molecules.[25, 26] We first characterized the binding property of avasimibe to HSA by circular dichroism (CD) and fluorescence spectroscopic analyses. As shown in Figure 1a, the CD spectra of HSA exhibited two negative bands in the ultraviolet region at 208 nm and 222 nm, which is characteristic of the α–helical structure of protein.[27, 28] By adding avasimibe, however, the intensities of the negative CD bands decreased notably, until the avasimibe:HSA molar ratio reached 33:1. The peak intensity change at 208 nm as a function of the avasimibe:HSA molar ratio was clearly shown (**Insert in** Figure 1a). This decrease in the α–helical content indicates the binding of avasimibe to HSA. Also, fluorescence quenching of the single tryptophan residue, Trp-214, (Figure S1a) suggests that the subdomain IIA of HSA is the avasimibe binding site.[29, 30] In addition, the magnitude of the intensity change suggests that at an avasimibe:HSA molar ratio of 16:1, the binding site is fully occupied by avasimibe. To further confirm the avasimibe binding site, warfarin was employed as a site I marker.[31] The binding site of warfarin to HSA was designated as site I, located in subdomain IIA near Trp-214.[32] Warfarin showed a fluorescence emission at 390 nm on excitation at 335 nm, and the addition of HSA (at warfarin:HSA molar ratio of 10:1) increased the fluorescence intensity due to warfarin binding to site I in the protein (Figure S1b). However, the addition of avasimibe (at avasimibe:HSA molar ratio of 16:1) caused the fluorescence of warfarin to return to its original intensity, indicating a complete replacement of warfarin by avasimibe at the primary binding site of HSA. This data suggests that the binding affinity of avasimibe to HSA is higher than that of warfarin ($1.89 \times 10^5\ M^{-1}$).[33] Collectively, these results show that avasimibe strongly binds to HSA and that the binding site is located in subdomain IIA.

Based on the above results, we prepared a water-soluble avasimibe formulation, referred to as avasimin, using a modified nanoencapsulation method.[34] The optimal loading amount of avasimibe was 10 wt % determined by a turbidity test of avasimin with different drug concentrations (Figure S2). The loading amount (10 wt %) of avasimibe in avasimin was further confirmed using HPLC analysis. The water-solubility of avasimibe and avasimin in PBS was compared using UV scattering at 430 nm (Figure 1b). The higher the UV scattering intensity, the more turbid the solution is. The turbidity measurement confirmed that the avasimin formulation increased the water-solubility of avasimibe by up to 10 times. The microscopic image of avasimibe solution showed undissolved and needle-shaped crystals of the drug, whereas the avasimin solution was clear (Figure S3). The TEM image permitted the visualization of the nano-sized and spherical morphology of avasimin. High-magnification TEM revealed HSA coating on the surface of avasimin (Figure 1c). In addition, the mean diameter, polydispersity, and surface charge of avasimin in PBS were

measured to be 169 nm, 0.41, and 0.83 mV, respectively (Figure S4). Together, these data demonstrate that the avasimin formulation effectively improved the water-solubility of the drug, thus allowing intravenous administration.

Cholesteryl ester depletion and cholesterol cytotoxicity in cancer cells induced by avasimin

We examined the accumulation of cholesteryl esters in lipid droplets in a panel of aggressive cancer cells and normal cells. By tuning the laser-beating frequency to be resonant with the C-H stretching vibration, substantial stimulated Raman loss (SRL) signals arose from intracellular lipid droplets.[35] The SRL images showed significant amounts of lipid droplets in various human cancer cells (PC3: Prostate cancer, MIA-PaCa2: Pancreatic cancer, A549: Lung cancer, HCT116: Colon cancer), whereas negligible amounts of lipid droplets in normal cells (hVSMC: Human vascular smooth muscle cells, BR5: Dermal fibroblast) were observed (Figure 2a,b). Notably, avasimin treatment reduced the amount of lipid droplets only in PC3 cells, but not in other cancer cells (Figure 2c). Next, we investigated the composition in lipid droplets using confocal Raman spectral analysis.[36] Raman spectra from different lipid droplets in the cancer cells were measured, and then the spectra were averaged to form a single spectrum. As shown in Figure 2d, the Raman spectrum of an lipid droplet in cancer cells exhibited the characteristic band for cholesterol ring vibration at 702 cm^{-1}.[37] The band at 702 cm^{-1} disappeared after avasimin treatment (**Green bar in** Figure 2d). To determine the cholesteryl ester molar percentage (%) in lipid droplets, the height ratio (I_{702}/I_{1442}) of the 702 cm^{-1} peak to the 1442 cm^{-1} peak (CH_2 bending) in the Raman spectra was calculated, and applied to the linear cholesteryl ester calibration curve obtained by the Raman spectra of cholesteryl ester/triacylglycerol emulsions with different cholesteryl ester/triacylglycerol molar ratios.[7] We found that cholesteryl esters predominated in lipid droplets for all cancer cell lines (PC3: 74±15 %, MIA-PaCa2: 61±15 %, A549: 52±18 %, HCT116: 57±13 %) (Figure 2e). Avasimin treatment significantly reduced the cholesteryl ester level in lipid droplets for all cancer cells. This cholesteryl ester depletion induced by avasimin was also confirmed using mass spectrometry measurement of cholesteryl esters in PC3 and MIA-PaCa2 cells (Figure S5).

We then investigated the anti-cancer effect of avasimin through cell viability measurement. The treatment of cancer and normal cells with avasimin at different concentrations selectively decreased the viability for cancer cells (Figure 3a). The half maximal inhibitory concentrations (IC_{50}) of avasimin for the cancer cells were significantly smaller than those for normal cells. We confirmed that this anti-cancer effect was not caused by HSA (Figure S6). Furthermore, by comparison with non-selective cytotoxic effects of conventional chemotherapeutics such as cisplatin and gemcitabine (Figure S7), the selective inhibitory effect of avasimin on cancer proliferation was clearly proved. To elucidate the inhibitory mechanism, we evaluated intracellular free cholesterol levels after avasimin treatment. As shown in Figure 3b, avasimin increased the amount of free cholesterol in the cancer cells by more than 50 %. In accordance, we observed a significant number of early and late apoptotic cells in the avasimin-treated group (Figure 3c,d). This apoptosis is likely induced by the high cholesterol level, which stiffens the endoplasmic reticulum (ER) membrane.[38, 39]

Collectively, these data show that avasimin selectively suppressed cancer proliferation by free cholesterol-mediated cytotoxicity.

Blood-residence time and tumor bioavailability of avasimibe following intravenous administration of avasimin

To measure the bioavailability of avasimibe in blood, avasimin (75 mg/kg, containing 7.5 mg/kg avasimibe) was administered to mice by tail vein injection. Avasimibe (15 mg/kg and 100 mg/kg) were also orally administered to mice as controls. By using liquid chromatography-mass spectroscopy (LC-MS), the plasma avasimibe concentration was measured as a function of time post-injection. A two-compartment pharmacokinetic model was used to fit the plasma concentration profile for intravenous administration of avasimin (Figure 4a and Table S1). The area under curve (AUC) of avasimibe for intravenous administration of avasimin was 136.36 μg·hr/ml, which was significantly larger than 14.92 μg·hr/ml and 49.9 μg·hr/ml for the oral administration of avasimibe at 15 mg/kg and 100 mg/kg, respectively. The distribution half-life and terminal half-life of avasimibe by intravenous administration of avasimin were 0.14 hr and 1.97 hr. These results show that avasimin effectively increased the blood-bioavailability of avasimibe.

Next, we characterized tissue distribution of avasimibe after intravenous administration of avasimin (75 mg/kg, containing 7.5 mg/kg avasimibe) and oral administration of avasimibe (15 mg/kg) to PC3 tumor-bearing mice. At 2 hr post administration, the concentrations of avasimibe in tissues, urine and feces were determined using LC-MS (Figure 4b). The tumor-bioavailability of avasimibe for intravenous administration of avasimin was 17.8 μg/g (34 μM, tumor density: 1.03 g/cm^3), which is 4-fold higher than the IC_{50} of the drug for PC3 cells (8.5 μM). In contrast, avasimibe was not detectable in the tumor tissue after oral administration. Orally administered drug is known to be absorbed by the gastrointestinal tract, and then carried to the liver through the hepatic portal vein.[40] Accordingly, most orally administered avasimibe was found in the liver tissue in which ACAT-1 was highly expressed (Figure 4b).[21] Also, in the oral administration group, a considerable amount of avasimibe was excreted through the feces. These results correspond to the low blood-bioavailability of avasimibe for the oral administration. Together, these results show that intravenous administration of avasimin significantly increased the drug concentration in the tumor by avoiding accumulation in the liver.

Anti-tumor activity of avasimin

The inhibitory activity of avasimin against subcutaneously xenografted PC3 and HCT116 tumors was evaluated. Avasimin (75 mg/kg, containing 7.5 mg/kg avasimibe) and PBS were intravenously administered daily for the first 5 days, followed by intravenous injection once every 4 days. In spite of the difference in growth profiles of PC3 and HCT116 tumors, avasimin notably inhibited both PC3 and HCT116 tumor growth, compared to the control groups that received PBS treatment (Figure 5a,b and Figure S8). Also, the avasimin treatment significantly extended the length of survival time in both tumor models (*P <0.005, by log-rank test). During the treatment, no obvious body weight change was observed (Figure S9). To evaluate the anti-tumor efficacy of oral avasimibe, we treated PC3 tumor xenografted mouse with avasimibe (15 mg/kg) daily using gavage feeding. However,

the orally administered avasimibe did not exhibit anti-tumor effect compared to the PBS treatment in terms of tumor volume (Figure S10).

We further studied the pharmacodynamics in both tumor models. SRL imaging showed a large amount of lipid accumulation in the tumor tissues (Figure 5c). Avasimin treatment distinctly reduced the amount of lipid droplets for the PC3 tumors, but not for the HCT116 tumors. Raman spectra from lipid droplets in the tumor tissues demonstrated the cholesterol ring vibration band at 702 cm^{-1} (**Green bar in** Figure 5d). The cholesteryl ester level (59±14 %) in lipid droplets of HCT116 tumor tissue was similar to *in vitro* cultured HCT116 cells (57±13 %), whereas the cholesteryl ester level (25±5 %) in lipid droplets of PC3 tumor tissue was smaller than that of cultured PC3 cells (74±15 %) (Figure 5e). This result suggests that different environmental conditions can alter lipid accumulation pathways in cancer cells. After repeated avasimin treatment, cholesteryl ester level (%) for both PC3 and HCT116 tumors were significantly reduced. The increase (more than 30 %) in free cholesterol levels for the tumor treated with avasimin was also determined (Figure 5f). In addition, TUNEL staining showed a significant number of apoptotic cells in the tumors treated with avasimin, compared to the tumors treated with PBS (Figure 5g, h). Collectively, the data demonstrate the potency of avasimin as a chemotherapeutic agent for various tumors.

In vivo safety evaluation

We evaluated *in vivo* toxicity of avasimin through hematological and histological analyses. Avasimin (75 mg/kg, containing 7.5 mg/kg avasimibe) was intravenously injected once every 4 days for 16 days (four injections in total). As a control group, PBS was administered in the same manner. The results of hematology and serum analyses between the avasimin-treated and PBS-treated groups were not significantly different, except for cholesterol levels (Figure 6a and Figure S11). The decrease in the blood cholesterol level in the avasimin-treated group was attributed to the reduction of very low density lipoprotein (VLDL) production in the liver mediated by ACAT-1 inhibition.[21] On the other hand, the levels of creatinine and alanine aminotransferase (ALT) for the avasimin-treated group were the same as those of the PBS-treated group, indicating no damage to the kidneys and the liver. The morphology of vital organs was assessed using H&E staining, and no morphological difference was observed between the groups treated with avasimin and PBS (Figure 6b). Furthermore, we investigated the influences of avasimin treatment to the lipid compositions in the liver and the adrenal glands, two key organs for lipid homeostasis[41] and cholesterol-based hormone synthesis.[42] Between the PBS-treated and avasimin-treated groups, the SRL images exhibited no difference in the amount of lipid droplets in the liver and the adrenal gland cortex (Figure 6c). Also, Raman spectra of lipid droplets were not significantly different between PBS-treated and avasimin-treated groups (Figure 6d). Interestingly, the Raman band at 702 cm^{-1} for the liver tissue was weak, whereas a strong band at 702 cm^{-1} for the adrenal gland tissue was observed (**Green bar in** Figure 6d). Our results support that the lipid droplets in the liver mainly have triacylglycerol (TG) by hepatic fatty acid *de novo* synthesis.[43] In contrast, the lipid droplets in the adrenal glands store a large amount of cholesteryl esters for steroid hormone synthesis.[42] Quantitation of the cholesteryl ester level

(Figure 6e) clearly showed no adverse effects of avasimin treatment to the adrenal glands. Together, these results demonstrate the safety of avasimin treatment in mouse models.

Discussion

One big challenge associated with cancer chemotherapy is non-specific toxicity to normal cells and organs.[44, 45] Conventional chemotherapeutic agents blocking DNA replication and cell division cause toxicity to both cancer and normal tissues.[46–48] Although advances in nanotechnology-based targeted drug delivery have improved the bioavailability of cytotoxic drugs at solid tumors, the majority of the drugs accumulate in normal tissues.[49–51] The toxicity of the drug delivery system has also been an issue.[52–54] The development of prodrugs activated by a cancer-specific enzyme or by the microenvironment has increased the selectivity of drugs.[55, 56] However, adverse effects by the inherent toxicity of the drugs are inevitable.[57–60] Targeting oncogenic protein kinase signaling pathways has reduced the off-targeting effect and non-specific toxicity.[61, 62] In spite of the benefits, the complicated therapeutic mechanism[63, 64] and the new adverse effects[65, 66] of targeted agents limit the clinical outcomes for cancer patients.[67, 68]

In this study, we demonstrated an effective approach for selective cancer chemotherapy by targeting the altered cholesterol metabolism in cancer cells. Although previous reports showed great anti-cancer potential of ACAT-1 inhibitors *in vitro*,[15, 16] there was no method to deliver a sufficient amount of inhibitor to the tumor *in vivo*. Furthermore, the pharmacokinetics and pharmacodynamics of the ACAT-1 inhibitor for cancer chemotherapy remain elusive. A major obstacle for delivering ACAT-1 inhibitor was its inherently low water-solubility.[19] Since all ACAT-1 inhibitors were previously administered orally to target hepatic lipoprotein (containing high cholesteryl esters) production for hypolipidemia and antherosclerosis treatments,[17] alternative routes for administration of the inhibitor have not been studied. By using highly biocompatible HSA, we developed a systemically injectable formulation of avasimibe (a potent ACAT-1 inhibitor), referred to as avasimin, for selective cancer chemotherapy. Through pharmacokinetic and pharmacodynamic studies using xenograft tumor models, we demonstrated that intravenous administration of avasimin not only significantly increased the bioavailability of avasimibe in the blood and the tumor by bypassing filtration through the liver, but also notably reduced cholesteryl esters in the tumor tissues. These results show the essentials of intravenous injectable formulation for avasimibe delivery in cancer chemotherapy.

We note that our method is applicable for other hydrophobic ACAT-1 inhibitors. By using interaction with HSA, systemically injectable formulations of various ACAT-1 inhibitors can be developed for effective cancer chemotherapy. Also, combination chemotherapy is viable based on our approach. Because HSA has multiple hydrophobic drug binding sites,[26] ACAT-1 inhibitor can be loaded with one or more chemo drugs into the nanoformulation. Cholesterol esterification blockade and free cholesterol elevation by ACAT-1 inhibitor can lead cancer cells to be more vulnerable to an existing chemotherapy, which may reduce not only the dose of the chemotherapy drug, but also associated toxicity. Thus, combination of an ACAT-1 inhibitor and an existing anti-cancer drug, both loaded into the HSA formulation, can significantly improve the outcome for cancer patients.

Conclusion

We developed a nano-formulation, termed avasimin, for intravenous delivery of avasimibe, a potent ACAT inhibitor, to aggressive tumors that store a large amount of cholesteryl ester in intracellular lipid droplets. In cultured cells, avasimin administration induced apoptosis to prostate, lung, colon and pancreatic cancer cells, but not to normal cells. In xenograph models of prostate cancer and colon cancer, intravenous administration of avasimin exhibited strong anti-cancer effect without toxicity to normal organs. These data together provide a new platform for treating aggressive cancer by targeting the altered cholesterol metabolism.

Experimental section

Characterization of interaction between avasimibe and HSA

Avasimibe solution (0–0.02 mg in 10 μl ethanol) was added to HSA solution (0.08 mg in 990 μl deionized water). The final molar concentrations of avasimibe and HSA were 0–40 μM and 1.2 μM, respectively. After incubation for 1 h at room temperature, circular dichroism (CD) spectra of the avasimibe-HSA solutions were measured using a JASCO J-810 spectropolarimeter (Tokyo, Japan) at 25 °C under a constant nitrogen flow. A quartz cell of 1 mm path length was used for spectrum measurement (190–260 nm). The spectra were collected with a data pitch of 1 nm, a scan speed of 10 nm per minute, and bandwidth of 1 nm. Each spectrum was the average of three scans.

To find the binding site of avasimibe on HSA, fluorescence emission spectrum change of tryptophan (Trp-214) in HSA by adding avasimibe was measured using a fluorescence spectrometer (SpectraMax M5, Molecular Devices, CA) with excitation at 280 nm and emission scanning from 300 nm to 450 nm at 25 °C.

Also, in order to determine the avasimibe binding to the drug binding site I on HSA, competitive binding assay using warfarin was performed.[29] Warfarin solution (0.004 mg in 10 μl ethanol) was mixed with HSA solution (0.08 mg in 980 μl deionized water), and the solution was incubated for 1 h at room temperature. Avasimibe (0.01 mg in 10 μl ethanol) was added to the warfarin-HSA solution. The warfarin, warfarin-HSA, warfarin-HSA +avasimibe solutions had the same mixed solvent composition of ethanol (20 μl) and water (980 μl). Fluorescence emission spectra of warfarin in the solutions were measured with excitation at 335 nm and emission scanning from 355 nm to 550 nm at 25 °C.

Formulation and characterization of avasimin

Avasimin was prepared using a modified nanoencapsulation method with HSA as a stabilizer.[34] In brief, avasimibe solution (1–2 mg in 1 ml ethanol) was added to HSA solution (4 mg in 4 ml PBS), and then the solution was incubated at 4 °C for 8 h. Untrapped avasimibe and ethanol were removed by dialysis (MWCO 12–14 kDa) against excess deionized water for 1 day and centrifugation (x1600 g, 10 min). The resulting solutions were lyophilized.

The loading amount of avasimibe in avasimin was measured by using liquid chromatography (LC) (Agilent 1200 HPLC). A Zorbax SB-C18 2.1×50mm, 1.8 μm column (Agilent) was used. The mobile phase consisted of water with 5 mM ammonium acetate (Buffer A) and 90 % acetonitrile with 5 mM ammonium acetate (Buffer B) was delivered at a flow rate of 0.3 ml/min. The sample injection volume was 10 μl. The retention time of the analyte (avasimibe) was 7.9 min.

The size distribution of avasimin (at 1 mg/ml PBS) was characterized using dynamic light scattering (DLS) (90Plus, Brookhaven Instruments Co., NY) at 633 nm at 25 °C. The zeta-potential of avasimin (at 1 mg/ml PBS) was also measured using a zeta-potential analyzer (ZetaPlus, Brookhaven Instruments Co., NY). The turbidities of avasimibe and avasimin solutions containing different concentrations of avasimibe (0–1 mg/ml PBS) were measured by UV absorption at 430 nm. The morphologies of avasimibe, avasimin, and HSA in PBS or distilled water were observed using an FV1000 confocal system (Olympus, Tokyo, Japan) and transmission electron microscopy (TEM) (CM200 electron microscope, Philips, OR).

Cell culture

Cells were cultured at 37 °C in a humidified atmosphere containing 5 % CO_2 and grown continuously in the following media: PC3 and A549 in F-12K supplemented with 10 % FBS, MIA-PaCa2 in RPMI1640 supplemented with 10 % FBS, HCT116 in McCoy's 5A supplemented with 10 % FBS, hVSMC in Medium 231 supplemented with 10 % FBS, and BR5 in DMEM supplemented with 10 % FBS. Coverslip-bottomed petri dishes (MatTek, Ashland, MA) were used for high-resolution imaging.

Label-free Raman spectromicroscopy

Label-free Raman spectromicroscopy was performed on live cells and tissue slices (~20 μm) without any staining process. SRL imaging was performed on a femtosecond SRL microscope, with the laser-beating frequency tuned to the C-H stretching vibration band at 2845 cm^{-1}, as described previously.[35] Compositional analysis of individual lipid droplets was performed by integration of high speed coherent anti-Stokes Raman scattering (CARS) imaging and confocal Raman spectral analysis on a single platform.[36] For CARS imaging and Raman spectra measurements of lipid droplets, the pump and Stokes lasers were tuned to 707 nm (14140 cm^{-1}) and 885 nm (11300 cm^{-1}), respectively, to be in resonance with the CH_2 symmetric stretch vibration.

With the SRL images, lipid droplet area (%) in a single cell was determined using ImageJ with "Threshold" and "Analyze Particles" functions. Raman spectra from different lipid droplets in the cancer cells were measured, and then the spectra were averaged to form a single spectrum. To determine cholesteryl ester molar percentage (%) in lipid droplets, the height ratio (I_{702}/I_{1442}) of the 702 cm^{-1} peak to the 1442 cm^{-1} peak in the Raman spectra was calculated, and the equation (I_{702}/I_{1442}=0.00255 × cholesteryl ester molar percentage (%)) generated from the cholesteryl ester calibration curve in our previous report[7] was employed.

Mass spectrometry measurement of cholesteryl esters

PC3 and MIA-PaCa2 cells were incubated with PBS and avasimin (25 μg/ml, containing 5 μM avasimibe) for 24 h. The cells were counted and collected by centrifugation. Lipid extraction from collected cell pellets was performed as reported previously.[69] In brief, the cells were re-suspended in 200 μl PBS. Methanol (1.5 ml) and chloroform (3 ml) were added to the cell solution, and incubated for 1 h at room temperature under gentle shaking. After adding water (1.25 ml), the solution was centrifuged (×1000 g, 10 min). The lower phase was collected and dried under vacuum. The sample was stored at −20 °C, and dissolved in 200 μl of chloroform/methanol/water (60:30:4.5, v/v/v) just before analysis. The lipid samples were mixed with ammonium acetate to form an ammonium adduct ions. Next, electrospray ionization mass spectrometry (ESI-MS) analysis was conducted according to the previous protocol.[70]

Free cholesterol quantification

The cells were incubated with PBS and avasimin (25 μg/ml, 5 μM avasimibe) for 48 h. The cells were counted and collected by centrifugation. For the tumor tissues, tumors were homogenized to make tissue solution. Lipids were extracted from the cell pellets and tumor tissue solutions as described above. Free cholesterol was quantified using a Cholesterol Quantitation Kit (Abcam).

Cell viability assay

The cells were incubated with PBS, avasimin (0–100 μg/ml, containing 0–20 μM avasimibe), HSA (80 μg/ml), cisplatin (0–40 μM), and gemcitabine (0–0.4 μM) for 72 h. Cell viability was measured by Thiazolyl Blue Tetrazolium Blue (MTT) colorimetric assay.

Fluorescent imaging of apoptotic cells

The cells were treated with PBS and avasimin (25 μg/ml, containing 5 μM avasimibe) for 48 h. Apoptotic cells were stained by Annexin V-FITC and propidium iodide (PI). Fluorescent imaging was performed using FV1000 confocal system (Olympus, Tokyo, Japan) equipped with Argon (488 nm) and HeNe (543 nm) lasers and a 40× water objective. Fluorescent images of apoptotic cells were acquired with 488 nm and 543 nm excitations and spectral filters of 500–530 nm and 555–655 nm for Annexin V-FITC and PI detections, respectively.

Animal models

All protocols for this animal study were approved by the Purdue Animal Care and Use Committee. PC3 or HCT116 cancer cells (2×10^6 cells) were mixed with an equal volume of Matrigel (BD Bioscience) and inoculated subcutaneously into the right flank of 6-week-old male athymic nude mice (Harlan Laboratories).

Bioavailability of avasimibe in blood and tissues

To compare the blood-bioavailability of avasimibe for oral and intravenous administrations, avasimibe solutions in PBS (15 mg/kg and 100 mg/kg) were orally administered to nude mice without tumors (n=3) using a plastic feeding tube (20 GA × 38 mm). Avasimin solution in PBS (75 mg/kg, containing 7.5 mg/kg avasimibe) was intravenously administered to nude

mice without tumor (n=3) through the tail vein. Blood samples (2 μl) were collected from the dorsal pedal vein at different time points post administration. The blood sample was mixed with K3-EDTA (0.2 μl, an anticoagulation agent), warfarin solution (5 ng in 1 μl deionized water, an internal standard), and DTT (40 μg in 0.5 μl PBS, a reducing agent). To extract avasimibe, acetone (6 μl) was added to the blood solution, vortexed, and then the solution was centrifuged (×5000 g, 5 min). The supernatant (6 μl) was collected and dried under vacuum. The sample was stored at −20 °C, and dissolved in 50 μl of methanol just before analysis. A linear standard curve of avasimibe in blood ranging of 0.01 – 100 μg/ml was created using the same extraction method described above. Avasimibe concentration was determined using a liquid chromatography-mass spectroscopy (LC-MS) (Agilent 1200 HPLC-Agilent 6460 QQQ mass spec). A Zorbax SB-C18 2.1×50mm, 1.8 μm column (Agilent) was used. The mobile phase consisted of water with 5 mM ammonium acetate (Buffer A) and 90 % acetonitrile with 5 mM ammonium acetate (Buffer B) was delivered at a flow rate of 0.3 ml/min. The sample injection volume was 10 μl. The retention times of the analyte (avasimibe) and the internal standard (warfarin) were 7.9 min and 6.6 min, respectively. To detect avasimibe, the mass spectrometer was operated in the multiple-reaction monitoring (MRM) mode, and was set to select the precursor-product ion transitions of m/z 500.1→177.0 and m/z 307.0→161.1 for avasimibe and warfarin, respectively.

The dataset was fit to a two-compartment pharmacokinetic model for avasimibe profile (R^2=0.99):

$$y = A_1 e^{(-x/t1)} + A_2 e^{(-x/t2)} + y_0$$

Based on this model, pharmacokinetic values for avasimibe delivered by intravenous administration of avasimin were determined including the initial volume of distribution, V_0:

$$V_0 = \text{Dose}/C_0\,(\text{initial concentration})$$

The plasma clearance, Cl_{Plasma}:

$$Cl_{\text{Plasma}} = V_0 \times k\,(\text{elimination rate constant})$$

The area under curve, AUC:

$$\text{AUC} = \text{Dose}/Cl_{\text{Plasma}}$$

The life-time for one-compartment model, $t_{1/2}$:

$$t_{1/2} = 0.693/k$$

The terminal half-time for two-compartment model, $t_{1/2,\,\text{term}}$:

$$t_{1/2,\ term} = 2\,Ln[2]/[k + k_{pt} + k_{tp} - ((k + k_{pt} + K_{tp})^2 - 4\,k\,k_{tp})^{0.5}]$$

And the distribution half-time for two-compartment model, $t_{1/2,\ dist}$:

$$t_{1/2,\ dist} = Ln[2]\,[k + k_{pt} + k_{tp} - ((k + k_{pt} + K_{tp})^2 - 4\,k\,k_{tp})^{0.5}]/[2\,k\,k_{tp}]$$

The terminal and distribution half-times for intravenous administration of avasimin were measured using the equations above, described in a previous report.[71]

To measure the bioavailability of avasimibe in tissues, avasimin solution in PBS (75 mg/kg, containing 7.5 mg/kg avasimibe) was intravenously administered to PC3 tumor xenograft nude mice (n=3) through the tail vein. Avasimibe solutions in PBS (15 mg/kg) was also orally administered to PC3 tumor xenograft nude mice (n=3). At 2 hr-post injection, the mice were sacrificed, and the tissues and urine were harvested and weighed. After adding PBS (100 μl per 100 μg tissue), the tissues were homogenized using a bead-based homogenizer (Precellys®24, Bertin Technologies). Avasimibe was extracted from the homogenized tissue solution according to the same procedure used in avasimibe extraction from blood sample. Avasimibe in the tissue, urine, and feces specimens was quantified by LC-MS using the same conditions as the blood-bioavailability study. The amounts of avasimibe were quantitatively determined based on the calibration curve of avasimibe in blood.

Anti-tumor effects

Anti-tumor effect of avasimin was evaluated by measuring the tumor volume and survival length. After reaching a tumor volume of 30–50 mm^3 14 and 7 days post PC3 and HCT116 cancer cell implantations respectively, PC3 and HCT116 tumor xenograft mice were randomized into two groups (n=8 per PBS or avasimin group). The mice received avasimin (75 mg/kg, containing 7.5 mg/kg avasimibe) and PBS by intravenous injection daily for the first 5 days, followed by intravenous injection once every 4 days. To evaluate the anti-tumor effect of oral avasimibe, the PC3 tumor xenografted mice were treated with avasimibe (15 mg/kg, in PBS) and PBS daily by gavage feeding (n=4 per PBS or avasimibe group). The body weight of the mice was monitored during the treatment. Tumor volume was measured as follows:

$$V = (a \times b^2)/2$$

where a and b represent the major and minor axes of a tumor, respectively. The lengths of the axes were measured using a caliper. When tumor volume reached over 10 % of body weight, mice were sacrificed and tumors were harvested for tissue analysis.

TUNEL and DAPI staining

The tumor tissues were fixed in 10 % neutral buffered formalin for at least 48 h, embedded into paraffin, sectioned at 5 μm thickness. The sections were stained with terminal deoxynucleotidyl transferase (TdT) and 4,6-diamidino-2-phenylindole (DAPI) according to the protocol of *in situ* cell death detection kit (Roche).

In vivo safety evaluation

Nude mice without tumors received avasimin (75 mg/kg, containing 7.5 mg/kg avasimibe) and PBS by intravenous injection once every 4 days for 16 days (four injections in total). The mice were sacrificed, blood and organs were collected. Complete blood count (CBC) and serum analyses were performed by Antech Diagnostics. The organs were fixed in 10 % neutral buffered formalin for at least 48 h, embedded into paraffin. Sections of 5 μm thickness were stained with hematoxylin and eosin in Purdue University Histopathology Lab. The slides were then examined on a Nikon microscope equipped with a charge-coupled device camera.

Statistical analysis

Statistic values are expressed as mean ± SD, and statistical comparisons between groups were made using one-way ANOVA and Student's t-test. For the Kaplan-Meier survival analysis, a log-rank test was performed. P value of <0.05 was considered statistically significant.

Supplementary Material

Refer to Web version on PubMed Central for supplementary material.

Acknowledgments

This work was supported by R01 CA129287 and DoD Prostate Cancer Research Program Idea Development Award. HPLC-MS data were acquired by a facility supported by P30 CA023168. The authors thank Dr. Shaoxiong Chen, pathologist in Indiana University School of Medicine, for examining the H&E stained tissues.

References

1. Vander Heiden MG, Cantley LC, Thompson CB. Understanding the Warburg Effect: The Metabolic Requirements of Cell Proliferation. Science. 2009; 324:1029–1033. [PubMed: 19460998]
2. Vander Heiden MG. Targeting Cancer Metabolism: A Therapeutic Window Opens. Nat Rev Drug Discov. 2011; 10:671–684. [PubMed: 21878982]
3. Zhao Y, Butler EB, Tan M. Targeting Cellular Metabolism to Improve Cancer Therapeutics. Cell Death Dis. 2013; 4:e532. [PubMed: 23470539]
4. Baenke F, Peck B, Miess H, Schulze A. Hooked on Fat: The Role of Lipid Synthesis in Cancer Metabolism and Tumour Development. Dis Model Mech. 2013; 6:1353–1363. [PubMed: 24203995]
5. Zhang F, Du G. Dysregulated Lipid Metabolism in Cancer. World J Biol Chem. 2012; 3:167–174. [PubMed: 22937213]
6. Nomura DK, Long JZ, Niessen S, Hoover HS, Ng SW, Cravatt BF. Monoacylglycerol Lipase Regulates a Fatty Acid Network that Promotes Cancer Pathogenesis. Cell. 2010; 140:49–61. [PubMed: 20079333]
7. Yue S, Li J, Lee SY, Lee Hyeon J, Shao T, Song B, Cheng L, Masterson Timothy A, Liu X, Ratliff Timothy L, et al. Cholesteryl Ester Accumulation Induced by PTEN Loss and PI3K/AKT Activation

Underlies Human Prostate Cancer Aggressiveness. Cell Metab. 2014; 19:393–406. [PubMed: 24606897]

8. Cruz PMR, Mo H, McConathy WJ, Sabins N, Lacko AG. The Role of Cholesterol Metabolism and Cholesterol Transport in Carcinogenesis: A Review of Scientific Findings, Relevant to Future Cancer Therapeutics. Front Pharmacol. 2013; 4:119. [PubMed: 24093019]
9. Ikonen E. Cellular Cholesterol Trafficking and Compartmentalization. Nat Rev Mol Cell Biol. 2008; 9:125–138. [PubMed: 18216769]
10. Tosi MR, Tugnoli V. Cholesteryl Esters in Malignancy. Clin Chim Acta. 2005; 359:27–45. [PubMed: 15939411]
11. Walther TC, Farese RVJ. Lipid Droplets and Cellular Lipid Metaoblism. Annu Rev Biochem. 2012; 81:587–714. [PubMed: 22482904]
12. Chang TY, Chang CCY, Ohgami N, Yamauchi Y. Cholesterol Sensing, Trafficking, and Esterificaiton. Annu Rev Cell Dev Biol. 2006; 22:129–157. [PubMed: 16753029]
13. de Medina P, Boubekeur N, Balaguer P, Favre G, Silvente-Poirot S, Poirot M. The prototypical Inhibitor of Cholesterol Esterification, Sah 58–035 [3-[Decyldimethylsilyl]-N-[2-(4-methylphenyl)-1-phenylethyl]propanamide], is an Agonist of Estrogen Receptors. J Pharmacol Exp Ther. 2006; 319:139–149. [PubMed: 16835370]
14. Paillasse MR, de Medina P, Amouroux G, Mhamdi L, Poirot M, Silvente-Poirot S. Signaling through Cholesterol Esterification: A New Pathway for the Cholecystokinin 2 Receptor Involved in Cell Growth and Invasion. J Lipid Res. 2009; 50:2203–2211. [PubMed: 19502590]
15. Bemlih S, Poirier MD, Andaloussi AE. Acyl-coenzyme A: Cholesterol Acyltransferase Inhibitor Avasimibe Affect Survival and Proliferation of Glioma Tumor Cell Lines. Cancer Biol Ther. 2010; 9:1025–1032. [PubMed: 20404512]
16. Antalis C, Arnold T, Rasool T, Lee B, Buhman K, Siddiqui R. High ACAT1 Expression in Estrogen Receptor Negative Basal-like Breast Cancer Cells is Associated with LDL-induced Proliferation. Breast Cancer Res Treat. 2010; 122:661–670. [PubMed: 19851860]
17. Farese RVJ. The Nine Lives of ACAT Inhibitors. Arterioscle Thromb Vasc Biol. 2006; 26:1684–1686.
18. Heinonen T. Inhibition of Acyl Coenzyme A-Cholesterol Acyltransferase: A Possible Treatment of Atherosclerosis? Curr Atheroscler Rep. 2002; 4:65–70. [PubMed: 11772425]
19. Chang TY, Li BL, Chang CCY, Urano Y. Acyl-coenzyme A:Cholesterol Acyltransferases. Am J Physiol Endocrinol Metab. 2009; 297:E1–E9. [PubMed: 19141679]
20. Homan R, Hamelehle KL. Influence of Membrane Partitioning on Inhibitors of Membrane-bound Enzymes. J Pharm Sci. 2001; 90:1859–1867. [PubMed: 11745743]
21. Burnett JR, Wilcox LJ, Telford DE, Kleinstiver SJ, Barrett PHR, Newton RS, Huff MW. Inhibition of ACAT by Avasimibe Decreases both VLDL and LDL Apolipoprotein B Production in Miniature Pigs. J Lipid Res. 1999; 40:1317–1327. [PubMed: 10393217]
22. Lee HT, Sliskovic DR, Picard JA, Roth BD, Wierenga W, Hicks JL, Bousley RF, Hamelehle KL, Homan R, Speyer C, et al. Inhibitors of Acyl- CoA:Cholesterol O-Acyl Transferase (ACAT) as Hypocholesterolemic Agents. CI-1011: An Acyl Sulfamate with Unique Cholesterol-Lowering Activity in Animals Fed Noncholesterol-Supplemented Diets. J Med Chem. 1996; 39:5031–5034. [PubMed: 8978833]
23. Robertson DG, Breider MA, Milad MA. Preclinical Safety Evaluation of Avasimibe in Beagle Dogs: An ACAT Inhibitor with Minimal Adrenal Effects. Toxicol Sci. 2001; 59:324–334. [PubMed: 11158726]
24. Llaverias G, Laguna JC, Alegret M. Pharmacology of the ACAT inhibitor Avasimibe (CI-1011). Cardiovascular Drug Reviews. 2003; 21:33–50. [PubMed: 12595916]
25. Ghuman J, Zunszain PA, Petitpas I, Bhattacharya AA, Otagiri M, Curry S. Structural Basis of the Drug-Binding Specificity of Human Serum Albumin. J Mol Biol. 2005; 353:38–52. [PubMed: 16169013]
26. Kratz F. Albumin as a Drug Carrier: Design of Prodrugs, Drug Conjugates and Nanoparticles. J Control Release. 2008; 132:171–183. [PubMed: 18582981]
27. Greenfield NJ. Using Circular Dichroism Spectra to Estimate Protein Secondary Structure. Nature Protoc. 2007; 1:2876–2890.

28. Ahmad B, Parveen S, Khan RH. Effect of Albumin Conformation on the Binding of Ciprofloxacin to Human Serum Albumin: A Novel Approach Directly Assigning Binding Site. Biomacromolecules. 2006; 7:1350–1356. [PubMed: 16602760]
29. Trynda-Lemiesz L. Paclitaxel–HSA Interaction. Binding Sites on HSA Molecule. Bioorg Med Chem. 2004; 12:3269–3275. [PubMed: 15158795]
30. Abou-Zied OK, Al-Shihi OIK. Characterization of Subdomain IIA Binding Site of Human Serum Albumin in Its Native, Unfolded, and Refolded States using Small Molecular Probes. J Am Chem Soc. 2008; 130:10793–10801. [PubMed: 18642807]
31. Dockal M, Chang M, Carter DC, Rüker F. Five Recombinant Fragments of Human Serum Albumin —Tools for the Characterization of the Warfarin Binding Site. Protein Sci. 2000; 9:1455–1465. [PubMed: 10975567]
32. He XM, Carter DC. Atomic Structure and Chemistry of Human Serum Albumin. Nature. 1992; 358:209–215. [PubMed: 1630489]
33. Vorum H, Honore B. Influence of Fatty Acids on the Binding of Warfarin and Phenprocoumon to Human Serum Albumin with Relation to Anticoagulant Therapy. J Pharm Pharmacol. 1996; 48:870–875. [PubMed: 8887741]
34. Pinto Reis C, Neufeld RJ, Ribeiro AJ, Veiga F. Nanoencapsulation I. Methods for Preparation of Drug-Loaded Polymeric Nanoparticles. Nanomedicine: Nanotechnology, Biology and Medicine. 2006; 2:8–21.
35. Zhang D, Slipchenko MN, Cheng JX. Highly Sensitive Vibrational Imaging by Femtosecond Pulse Stimulated Raman Loss. J Phys Chem Lett. 2011; 2:1248–1253. [PubMed: 21731798]
36. Slipchenko MN, Le TT, Chen H, Cheng JX. High-speed Vibrational Imaging and Spectral Analysis of Lipid Bodies by Compound Raman Microscopy. J Phys Chem B. 2009; 113:7681–7686. [PubMed: 19422201]
37. Movasaghi Z, Rehman S, Rehman IU. Raman Spectroscopy of Biological Tissues. Appl Spectrosc Rev. 2007; 42:493–541.
38. Kellner-Weibel G, Jerome WG, Small DM, Warner GJ, Stoltenborg JK, Kearney MA, Corjay MH, Phillips MC, Rothblat GH. Effects of Intracellular Free Cholesterol Accumulation on Macrophage Viability: A Model for Foam Cell Death. Arterioscler Thromb Vasc Biol. 1998; 18:423–431. [PubMed: 9514411]
39. Maxfield FR, Tabas I. Role of Cholesterol and Lipid Organization in Disease. Nature. 2005; 438:612–621. [PubMed: 16319881]
40. El-Kattan, A., Varma, M. Oral Absorption, Intestinal Metabolism and Human Oral Bioavailability. In: James, P., editor. Topics on drug metabolism. InTech; 2012. http://dx.doi.org/10.5772/31087
41. Nguyen P, Leray V, Diez M, Serisier S, Bloc'h JL, Siliart B, Dumon H. Liver Lipid Metabolism. J Anim Physiol Anim Nutr. 2008; 92:272–283.
42. Ghayee H, Auchus R. Basic Concepts and Recent Developments in Human Steroid Hormone Biosynthesis. Rev Endocr Metab Disord. 2007; 8:289–300. [PubMed: 17926129]
43. Jensen-Urstad APL, Semenkovich CF. Fatty Acid Synthase and Liver Triglyceride Metabolism: Housekeeper or Messenger? Biochim Biophys Acta. 2012; 1821:747–753. [PubMed: 22009142]
44. Laviano A, Rossi Fanelli F. Toxicity in Chemotherapy-when Less is More. N Engl J Med. 2012; 366:2319–2320. [PubMed: 22694004]
45. Norris RE, Adamson PC. Challenges and Opportunities in Childhood Cancer Drug Development. Nature Rev Cancer. 2012; 12:776–782. [PubMed: 23051845]
46. Lucas D, Scheiermann C, Chow A, Kunisaki Y, Bruns I, Barrick C, Tessarollo L, Frenette PS. Chemotherapy-Induced Bone Marrow Nerve Injury Impairs Hematopoietic Regeneration. Nature Med. 2013; 19:695–703. [PubMed: 23644514]
47. Monsuez JJ, Charniot JC, Vignat N, Artigou JY. Cardiac Side-Effects of Cancer Chemotherapy. Int J Cardiol. 2010; 144:3–15. [PubMed: 20399520]
48. Torino F, Barnabei A, De Vecchis L, Sini V, Schittulli F, Marchetti P, Corsello SM. Chemotherapy-Induced Ovarian Toxicity in Patients Affected by Endocrine-Responsive Early Breast Cancer. Crit Rev Oncol Hematol. 2014; 89:27–42. [PubMed: 23953684]
49. Park K. Facing the Truth about Nanotechnology in Drug Delivery. ACS Nano. 2013; 7:7442–7447. [PubMed: 24490875]

50. Cabral H, Matsumoto Y, Mizuno K, Chen Q, Murakami M, Kimura M, Terada Y, Kano MR, Miyazono K, Uesaka M, et al. Accumulation of Sub-100 nm Polymeric Micelles in Poorly Permeable Tumours Depends on Size. Nature Nanotech. 2011; 6:815–823.
51. Namgung R, Mi Lee Y, Kim J, Jang Y, Lee BH, Kim IS, Sokkar P, Rhee YM, Hoffman AS, Kim WJ. Poly-Cyclodextrin and Poly-Paclitaxel Nano-Assembly for Anticancer Therapy. Nat Commun. 2014; 5:3702. [PubMed: 24805848]
52. Vega-Villa KR, Takemoto JK, Yáñez JA, Remsberg CM, Forrest ML, Davies NM. Clinical Toxicities of Nanocarrier Systems. Adv Drug Deliv Rev. 2008; 60:929–938. [PubMed: 18313790]
53. Jong WHD, Borm PJ. Drug Delivery and Nanoparticles: Applications and Hazards. Int J Nanomedicine. 2008; 3:133–149. [PubMed: 18686775]
54. Igarashi E. Factors Affecting Toxicity and Efficacy of Polymeric Nanomedicines. Toxicol Appl Pharmacol. 2008; 229:121–134. [PubMed: 18355886]
55. Rautio J, Kumpulainen H, Heimbach T, Oliyai R, Oh D, Jarvinen T, Savolainen J. Prodrugs: Design and Clinical Applications. Nature Rev Drug Discov. 2008; 7:255– 270. [PubMed: 18219308]
56. Huttunen KM, Raunio H, Rautio J. Prodrugs-From Serendipity to Rational Design. Pharmacol Rev. 2011; 63:750–771. [PubMed: 21737530]
57. Endo A, Yoshida Y, Nakashima R, Takahashi N, Tanabe K. Capecitabine Induces both Cardiomyopathy and Multifocal Cerebral Leukoencephalopathy. Int Heart J. 2013; 54:417–420. [PubMed: 24309454]
58. Lee AE, Wilson WR. Hypoxia-Dependent Retinal Toxicity of Bioreductive Anticancer Prodrugs in Mice. Toxicol Appl Pharmacol. 2000; 163:50–59. [PubMed: 10662604]
59. Prijovich ZM, Chen BM, Leu YL, Chern JW, Roffler SR. Anti-Tumour Activity and Toxicity of the New Prodrug 9-Aminocamptothecin Glucuronide (9ACG) in Mice. Br J Cancer. 2002; 86:1634–1638. [PubMed: 12085215]
60. Tang MHY, Helsby NA, Goldthorpe MA, Thompson KM, Al-Ali S, Tingle MD. Hepatic Nitroreduction, Toxicity and Toxicokinetics of the Anti-Tumour Prodrug CB 1954 in Mouse and Rat. Toxicology. 2007; 240:70–85. [PubMed: 17804142]
61. Sebolt-Leopold JS, English JM. Mechanisms of Drug Inhibition of Signalling Molecules. Nature. 2006; 441:457–462. [PubMed: 16724058]
62. Zhang J, Yang PL, Gray NS. Targeting Cancer with Small Molecule Kinase Inhibitors. Nature Rev Cancer. 2009; 9:28–39. [PubMed: 19104514]
63. O'Reilly KE, Rojo F, She QB, Solit D, Mills GB, Smith D, Lane H, Hofmann F, Hicklin DJ, Ludwig DL, et al. mTOR Inhibition Induces Upstream Receptor Tyrosine Kinase Signaling and Activates Akt. Cancer Res. 2006; 66:1500–1508. [PubMed: 16452206]
64. Carracedo A, Ma L, Teruya-Feldstein J, Rojo F, Salmena L, Alimonti A, Egia A, Sasaki AT, Thomas G, Kozma SC, et al. Inhibition of mTORC1 Leads to MAPK Pathway Activation through a PI3K-Dependent Feedback Loop in Human Cancer. J Clin Invest. 2008; 118:3065–3074. [PubMed: 18725988]
65. Choueiri TK, Mayer EL, Je Y, Rosenberg JE, Nguyen PL, Azzi GR, Bellmunt J, Burstein HJ, Schutz FAB. Congestive Heart Failure Risk in Patients with Breast Cancer Treated with Bevacizumab. J Clin Oncol. 2011; 29:632–638. [PubMed: 21205755]
66. Belum VR, Fontanilla Patel H, Lacouture ME, Rodeck U. Skin Toxicity of Targeted Cancer Agents: Mechanisms and Intervention. Future Oncol. 2013; 9:1161–1170. [PubMed: 23902247]
67. Keefe DMK, Bateman EH. Tumor Control *versus* Adverse Events with Targeted Anticancer Therapies. Nature Rev Clin Oncol. 2012; 9:98–109.
68. Awada A, Aftimos PG. Targeted Therapies of Solid Cancers: New Options, New Challenges. Curr Opin Oncol. 2013; 25:296–304. [PubMed: 23493191]
69. Yang WC, Adamec J, Regnier FE. Enhancement of the LC/MS Analysis of Fatty Acids through Derivatization and Stableisotope Coding. Anal Chem. 2007; 79:5150–5157. [PubMed: 17492837]
70. Liebisch G, Binder M, Schifferer R, Langmann T, Schulz B, Schmitz G. High throughput Quantification of Cholesterol and Cholesteryl Ester by Electrospray Ionization Tandem Mass Spectrometry (ESI-MS/MS). Biochim Biophys Acta. 2006; 1761:121–128. [PubMed: 16458590]

71. Lee S-Y, Kim S, Tyler JY, Park K, Cheng J-X. Blood-Stable, Tumor-Adaptable Disulfide Bonded mPEG-(Cys)4-PDLLA Micelles for Chemotherapy. Biomaterials. 2013; 34:552–561. [PubMed: 23079665]

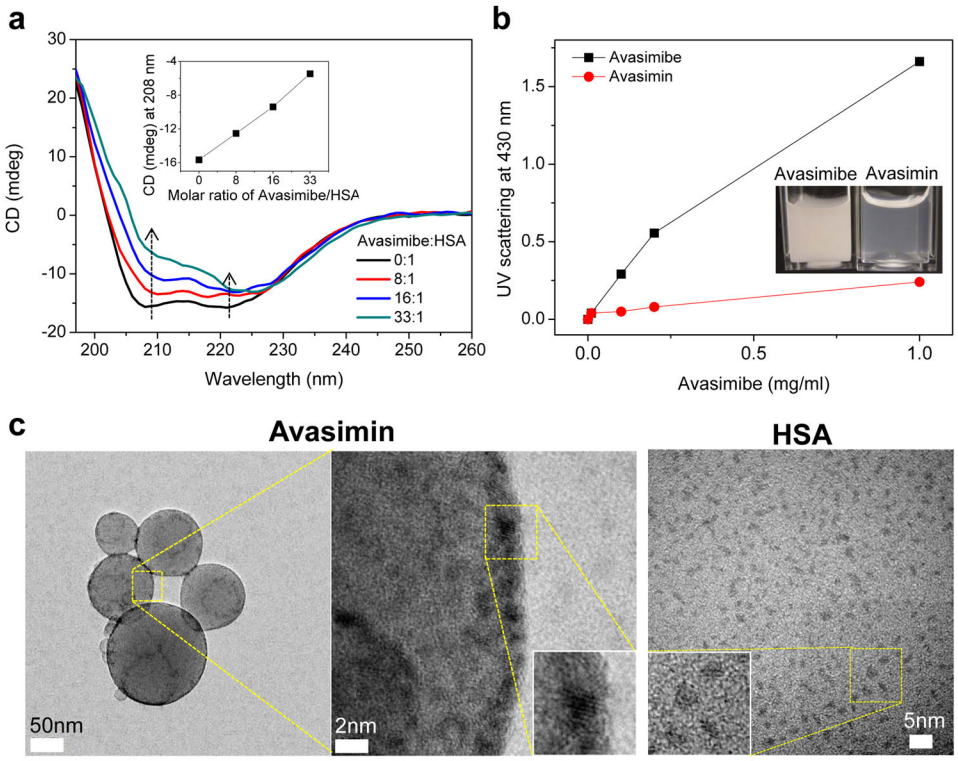

Figure 1.

Water-soluble avasimibe nanomedicine, avasimin. (a) CD spectra of HSA at different avasimibe:HSA molar ratios. Insert: Plot of CD intensity at 208 nm as a function of avasimibe/HSA molar ratio. (b) Solubility measurement of avasimibe and avasimin (with 10 wt % avasimibe loading) in PBS by UV scattering at 430 nm. Insert photograph shows avasimibe (1 mg/ml) and avasimin containing the same concentration of avasimibe in PBS. (c) High-magnification TEM images of avasimin and HSA. The size, polydispersity, and zeta-potential of avasimin are 169 ± 85 nm, 0.41, and 0.83 ± 4.95 mV, respectively.

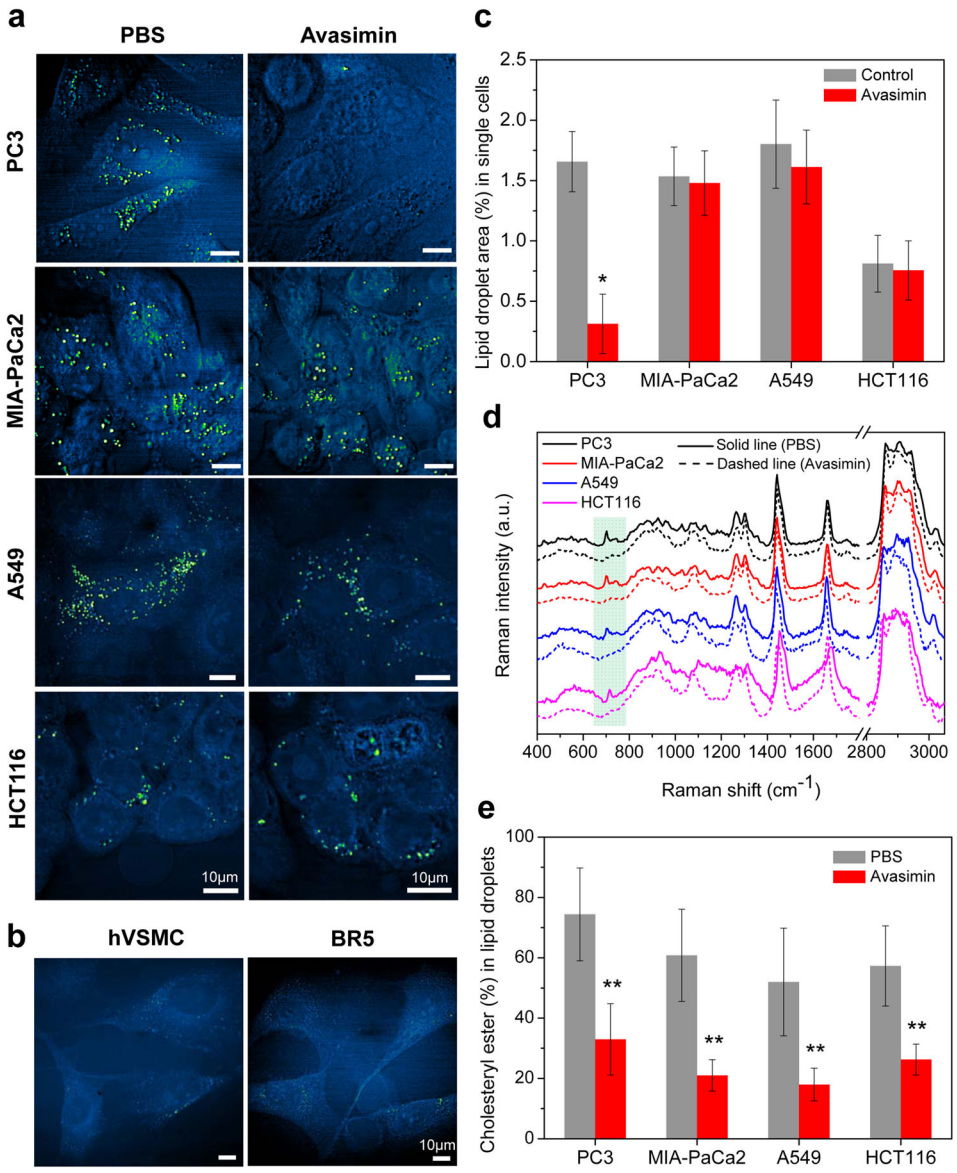

Figure 2.

Avasimin inhibits storage of cholesteryl ester in various human cancer cells. (a–b) SRL images of (a) various human cancer cells (PC3: Prostate cancer, MIA-PaCa2: Pancreatic cancer, A549: Lung cancer, HCT116: Colon cancer) treated with avasimin (25 μg/ml, containing 5 μM avasimibe) and with PBS as a control for 24 hr, and (b) normal human cells without treatment (hVSMC: Vascular smooth muscle, BR5: Dermal fibroblast). (c) Quantification of lipid droplet area (%) in single cells in (a) (n=20). $*P < 0.001$. (d) Raman spectra of lipid droplets in cancer cells shown in (a). Green bar indicates the Raman band of cholesterol at 702 cm^{-1} (n=5 to 10). Solid and dashed lines represent groups treated with PBS and avasimin, respectively. (e) Quantification of cholesteryl ester molar percentage (%) in lipid droplets based on the Raman spectra in (d) (n=5 to 10). $**P < 0.05$. Data are expressed as mean ± SD.

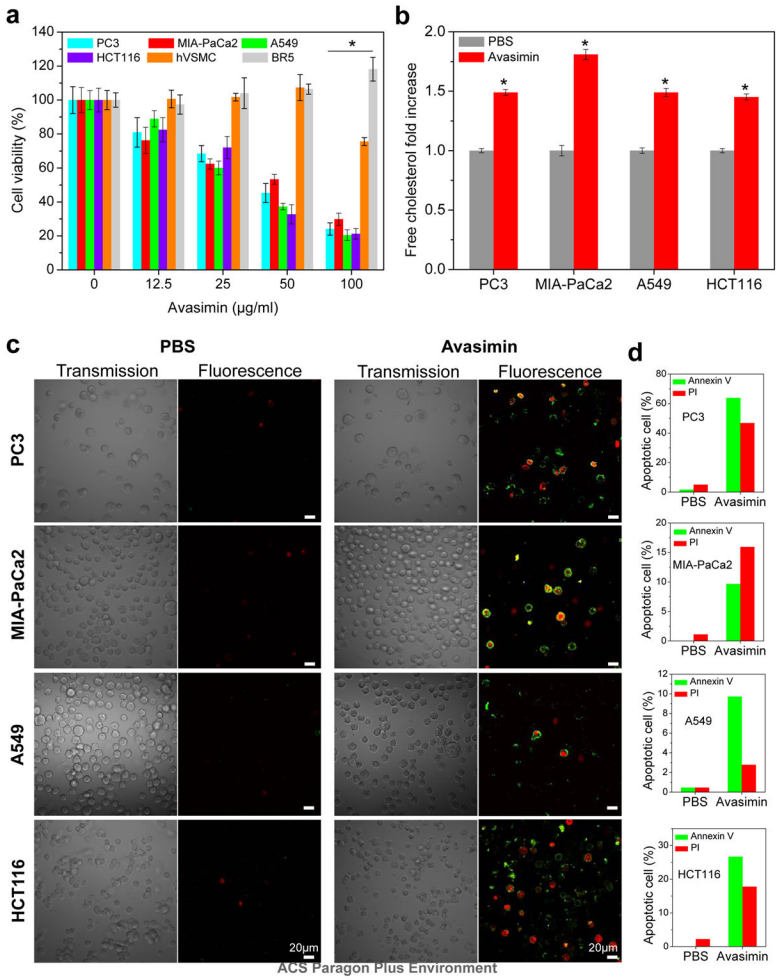

Figure 3.

Avasimin induces cancer-selective cholesterol cytotoxicity. (a) Cell viability assay. Cell viability was determined following treatment of avasimin at different concentrations (0–100 μg/ml, containing 0–20 μM avasimibe) for 72 h (n=8). **P* < 0.001. IC_{50} values of avasimin (containing avasimibe, μM) are 21 μg/ml (8.5 μM) for PC3, 22.5 μg/ml (9 μM) for MIA-PaCa2, 19.5 μg/ml (7.8 μM) for A549, 18.7 μg/ml (7.5 μM) for HCT116, 118.7 μg/ml (47.5 μM) for hVSMC, and 126.3 μg/ml (50 μM) for BR5. (b) Free cholesterol amount in cancer cells treated with avasimin (25 μg/ml, containing 5 μM avasimibe) and with PBS as a control for 48 hr. The amount of free cholesterol was normalized by the control group of each cancer cell line (n=4). **P* < 0.001. Data are expressed as mean ± SD. (c) Fluorescent imaging of apoptotic cells. The cells were incubated with avasimin (25 μg/ml, containing 5 μM avasimibe) and with PBS as a control for 48 hr. The green and red fluorescence represent Annexin V and PI, respectively. (d) Quantification of apoptotic cells (%). Annexin V and PI positive cells represent early and late apoptotic cells, respectively.

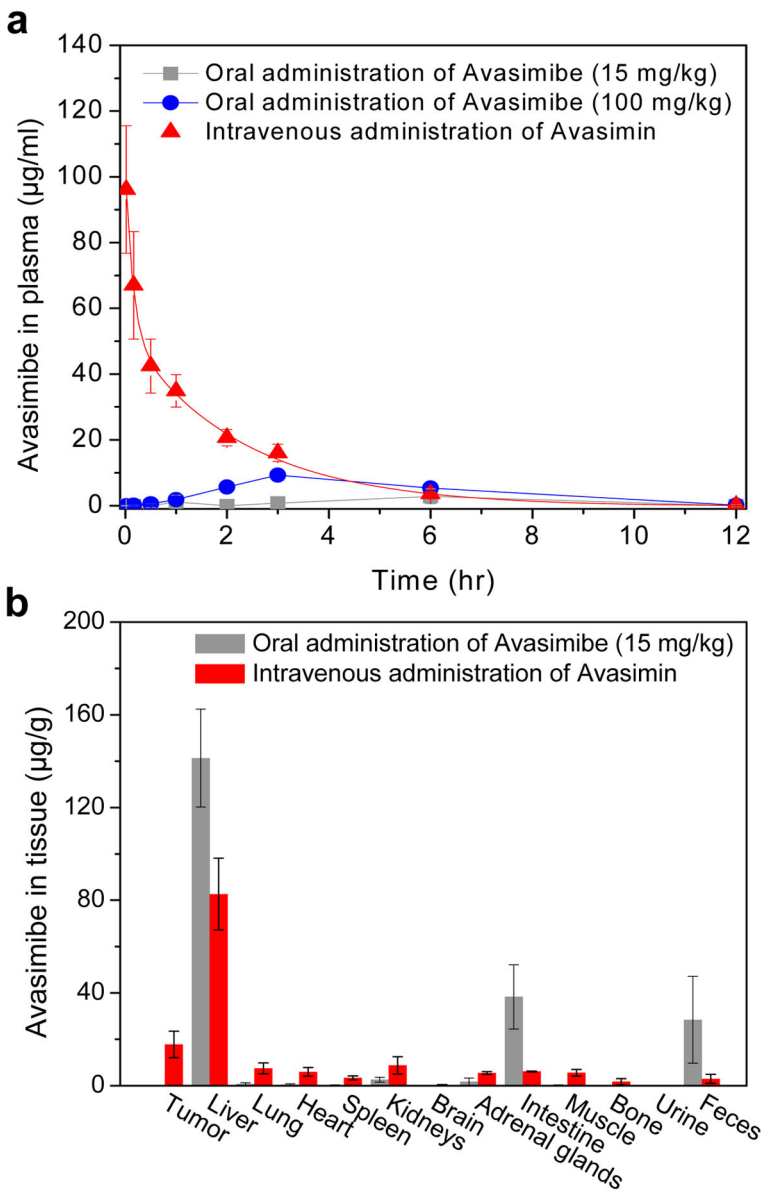

Figure 4.

Avasimin improves bioavailability of avasimibe in blood and tumor by intravenous administration. (a) Blood bioavailability of avasimibe following intravenous administration of avasimin (75 mg/kg, containing 7.5 mg/kg avasimibe) or oral administration of avasimibe (15 mg/kg and 100 mg/kg) (n=3 for each group). The avasimibe profile for intravenous administration of avasimin was fitted with a two-compartment model ($y = A_1 e^{(-x/t1)} + A_2 e^{(-x/t2)} + y_0$). (b) Tissue distribution of avasimibe at 2 hr after intravenous injection of avasimin (75 mg/kg, containing 7.5 mg/kg avasimibe) or oral administration of avasimibe (15 mg/kg) (n=3 for each group). Data are expressed as mean ± SD.

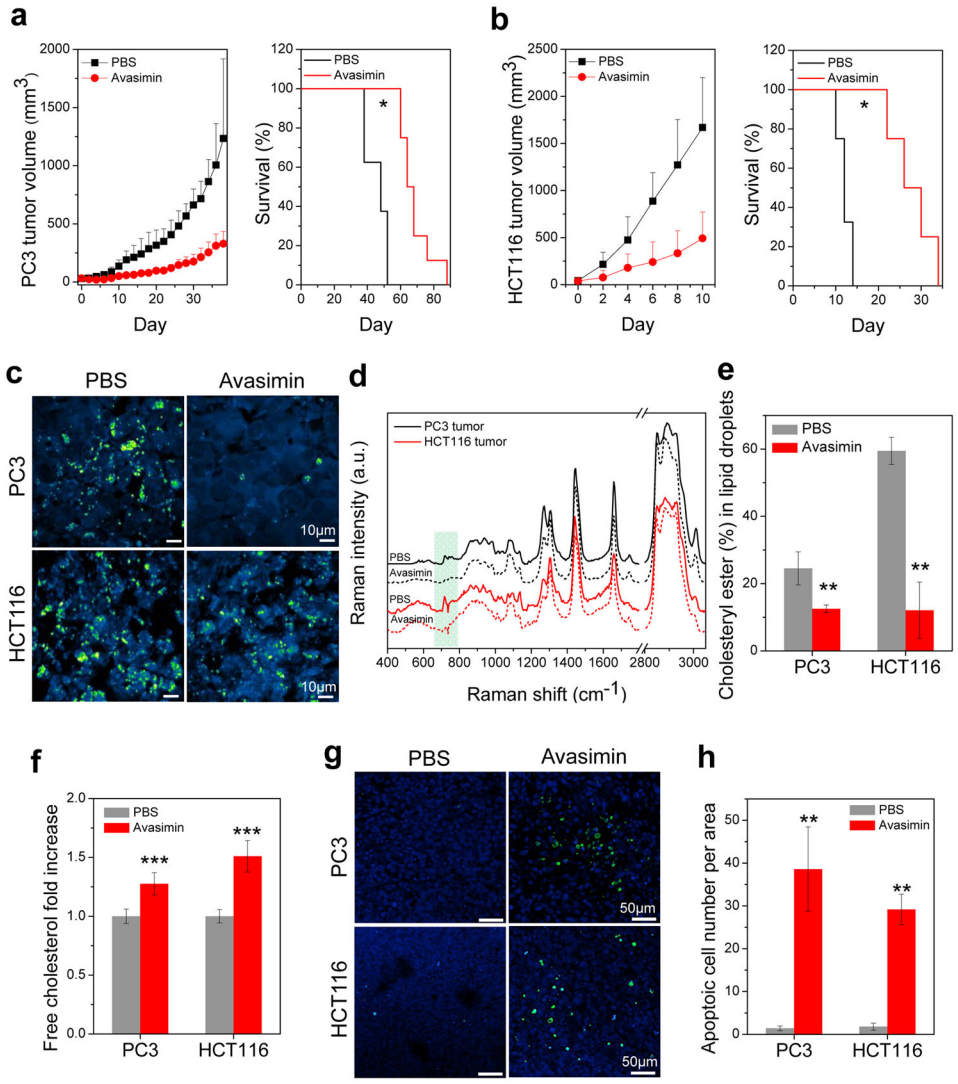

Figure 5.

Anti-tumor effects of avasimin for PC3 and HCT116 tumor xenograft mouse models. (a–b) Tumor volume (left) and survival rate (right) of (a) PC3 and (b) HCT116 tumor xenograft mice (n=8 for each group). The mice received avasimin (75 mg/kg, containing 7.5 mg/kg avasimibe) or PBS by intravenous injection daily for the first 5 days, following by intravenous injection once every 4 days. Day was counted after post initial treatment. $*P < 0.005$ (log-rank test). (c) SRL images of PC3 and HCT116 tumor tissues. (d) Raman spectra of lipid droplets in the tissues shown in (c). Green bar indicates the Raman band of cholesterol at 702 cm^{-1}. Solid and dashed lines represent groups treated with PBS and avasimin, respectively. (e) Quantification of cholesteryl ester molar percentage (%) in lipid droplets based on the Raman spectra in (d) (n=5 to 10). (f) Free cholesterol increase in the tumor tissues (n=4). (g) Tumor tissue stained with TUNEL and DAPI. Fluorescence blue and green indicate DAPI (cell nucleus, blue fluorescence) and TUNEL (apoptotic cells, green fluorescence) signals, respectively. (h) Quantification of TUNEL positive cells

(apoptotic cells) in the tumor tissues shown in (g) (n=5). $^{**}P < 0.005$, $^{***}P < 0.01$. Data are expressed as mean ± SD.

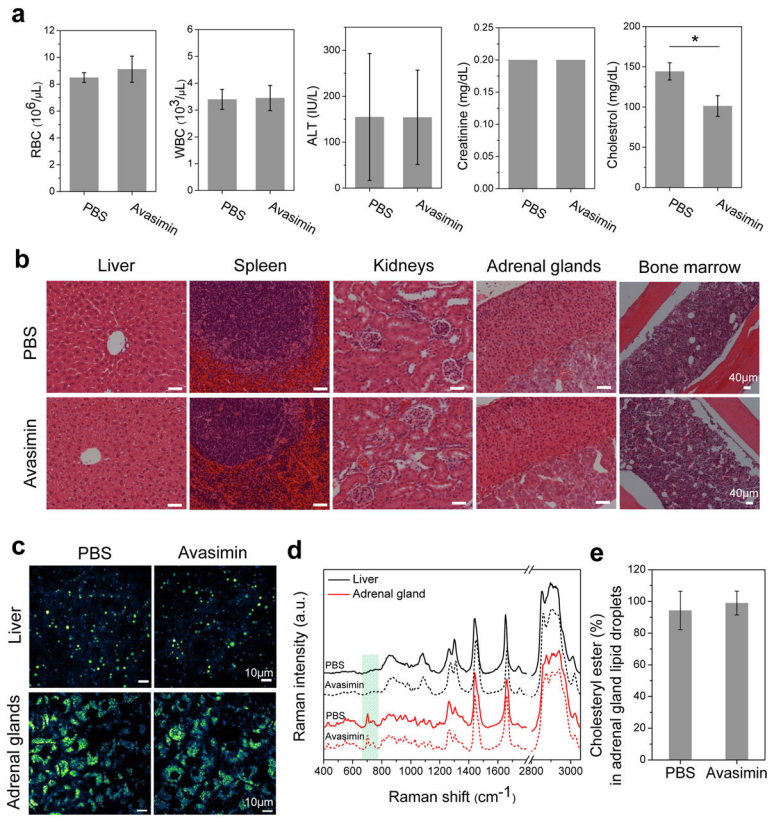

Figure 6.

In vivo safety assay. (a) Complete blood count (CBC) and serum analyses of mouse after intravenous injection of avasimin (75 mg/kg, containing 7.5 mg/kg avasimibe) or PBS once every 4 days for 16 days (four injections in total) (n=3). $*P < 0.05$. (b) Histological analysis explanted liver, spleen, kidneys, adrenal glands, and bone marrow stained with hematoxylin and eosin. (c) SRL images of lipids in liver and adrenal gland cortex tissues. (d) Raman spectra of lipid droplets in the tissues shown in (c). Green bar indicates the Raman band of cholesterol and at 702 cm^{-1} (n=5 to 10). Solid and dashed lines represent groups treated with PBS and avasimin, respectively. (e) Quantification of cholesteryl ester molar percentage (%) in lipid droplets in adrenal glands based on the Raman spectra in (d) (n=5 to 10). Data are expressed as mean ± SD.